International Journal of Concrete Structures and Materials

RESEARCH

Open Access

Proposal of a Creep-Experiment Method and Superficial Creep Coefficient Model of CFT Considering a Stress-Redistribution Effect

Yu-A. Kim[1], Jung-Soo Lee[2], Seung-Hee Kwon[3] and Jin-Kook Kim[1*]

Abstract

Existing concrete creep coefficient prediction models have the limitation of not considering the structural characteristics of CFT. For this reason, these models tend to overestimate the creep deformation of CFT. Therefore, in order to overcome the limitations of existing CFT creep experiments, this study proposes a creep-experiment method involving the use of CFT that passively changes the load applied to a single concrete specimen by calculating the stress redistribution between the concrete and a steel tube in CFT based on a step-by-step method. Furthermore, by actually applying the proposed experimental method, a creep experiment of CFT lasting for approximately 163 days was performed and a superficial creep coefficient model of CFT was proposed based on long-term strain data from the experiment. In order to verify the proposed superficial creep coefficient model, it was compared with two design criteria (CEB-FIP and ACI) based on the experimental results of this study and references. As a result, compared to the existing design criteria, the value predicted by the proposed superficial creep coefficient model showed good agreement with the experimental results of this study and the references, proving that the proposed creep-experiment method of CFT and superficial creep coefficient model are reasonable.

Keywords CFT, Creep-experiment method, Superficial creep coefficient, Stress redistribution, Step-by-step method

1 Introduction

The concrete-filled steel tube (CFT) is a composite structure made with concrete filled into a round or square steel tube. Such tubes show excellent structural performance by maximizing the advantages of both materials. The lateral deformation of concrete is restrained by the steel tube, which can have the effect of enhancing the strength, and due to the concrete inside, the steel tube can overcome the material limitation of being vulnerable to buckling. However, when a load is applied, CFT causes different levels of deformation in concrete and steel tubes over time due to the long-term behavioral characteristics of the internal concrete (Kwon et al., 2005; Wang & Zhao, 2018; Wang et al., 2019). Such unequal deformation may adversely affect the durability of the structure by generating unnecessary stress at the joints of the structure. The drying shrinkage and dry creep of CFT is greatly reduced compared to that of general concrete because contact between the concrete and the outside air is blocked by the steel tube (Lai et al., 2019; Nakai et al., 1991; Zhang et al., 2015). In addition, a stress-redistribution effect occurs between the two materials of the CFT because the steel tube additionally receives the stress loss caused by creep in the concrete while the CFT behaves integrally. Although slips phenomenon may occur

Journal information: ISSN 1976-0485 / eISSN 2234-1315.

*Correspondence:
Jin-Kook Kim
jinkook.kim@seoultech.ac.kr
[1] Department of Civil Engineering, Seoul National University of Science and Technology, 232 Gongneung-Ro, Nowon-Gu, Seoul 01811, Republic of Korea
[2] Hybrid Structural Testing Center, Myongji University, 34 Geobukgol-Ro, Seodaemun-Gu, Seoul 17060, Republic of Korea
[3] Department of Civil and Environmental Engineering, Myongji University, 34 Geobukgol-Ro, Seodaemun-Gu, Seoul 17060, Republic of Korea

between concrete and steel tube, this study assumes integral behavior between the two materials to analyze the superficial creep behavior due to the effect of stress redistribution. As such, because the long-term behavior characteristics of CFT differ from those of general concrete, in order to secure the stability and proper maintenance of structures using CFT, it is necessary closely to analyze the time-dependent behavior with regard to the structural characteristics of the CFT.

In order to predict the long-term deformation of CFT, various studies of the long-term behavioral characteristics of CFT have been conducted by many researchers. Chen et al. (Chen et al., 2017) evaluated the predictive performance of four creep models (CEB-FIP (CEB-FIP., 1993), fib MC2010 (fib., 2010), ACI (Committee&209.,), and B4 (Bažant & Wan-Wendner, 2015)) based on experiments on 13 specimens and 35 experimental data points in the literature to evaluate the creep behavior of CFT; the temporal behavior of a CFT arch bridge was evaluated by applying the model with the best predictive performance. As a result, the ACI 209 (Committee&209.,) model was found to predict the creep behavior better than other models, but the predictive performance of the creep model differed depending on the variables of the experimental data. The conclusion was that it is impossible to propose the most suitable model for CFT. Nguyen et al. (Nguyen et al., 2021) conducted a creep experiment on normal concrete and CFT specimens over a period of 400 days to study the effect of the redistribution of the stress between the steel tube and concrete caused by creep, where the predicted values of creep deformation in creep models [B4 (Bažant & Wan-Wendner, 2015), B4-TW (Chin, 2017; Liu, 2017)] were compared with experimental data. As a result, the loading day according to the age of concrete had the greatest effect on the basic creep, with the creep and shrinkage strain of the CFT specimen being 33% and 62% lower, respectively, compared to a general concrete specimen. In addition, for the CFT specimen, the stress in the steel tube increased by approximately 33%, while the stress in the concrete decreased by about 16% at 375 days due to the stress-redistribution effect. The B4-TW (Chin, 2017; Liu, 2017) model had better creep deformation prediction performance than the B4 (Bažant & Wan-Wendner, 2015) model, but the values predicted by both models tended to be too high compared to the actual experimental data. Yi et al. (Yi & Yuan, 2012) studied the creep behavior of CFT for 380 days with four CFT specimens (HCFT) using high-strength concrete. The creep coefficient of their high-strength concrete-filled (HCFT) specimen was lower by about 15% compared to a CFT specimen filled with normal-strength concrete. Based on these experimental results, a modified B3 (Baweja & Bažant, 1995) model was proposed based on a regression equation to propose a reasonable HCFT creep model. Wang et al. (Wang et al., 2011) conducted an experiment involving different loading days and axial load levels on 11 short expanded concrete-filled steel tube (ECFST) specimens to provide experimental data pertaining to the temporal behavior of ECFST, studies of which are relatively rare. The accuracy rates of four creep models (Eurocode 2 (BS EN, 2004), fib MC 2010 (fib., 2010), AFREM (Roy et al., 1996), B3 (Baweja & Bažant, 1995)) were evaluated based on the experimental data. As a result, it was recommended to use the Eurocode 2 (BS EN, 2004) model to predict the long-term behavior of ECFST specimens.

However, studies of methods that can be used to predict the long-term behavior of CFT are still insufficient. Most of the design criteria currently used to predict creep deformation are empirical equations derived based on experimental data on the long-term behavior of concrete. Therefore, existing design criteria overestimate the creep deformation of CFT because they do not reflect structural characteristics of CFT such as blocking drying shrinkage and stress redistribution effects. For these reasons, in order to predict the creep deformation of CFT accurately, a creep model capable of properly reflecting the long-term behavior characteristics of CFT must be devised. However, for CFT, of which relatively few long-term experimental datasets exist compared to concrete, creep prediction models are extremely rare. One of the reasons for the lack of research involving creep experiments on CFT is that devising a long-term behavior experimental method for CFT is more difficult than doing so for general concrete due to the structural characteristics of the concrete filling the steel tube. When the height of the concrete and the steel tube are different, it is difficult to accurately pressurize the two materials simultaneously. In addition, there is a high possibility of errors in the process of measuring the creep strain of internal concrete. It is also difficult to diversify certain design parameters, such as the steel ratio, because the manufacturing process of these types of specimens is complicated. Therefore, in order to perform CFT creep experiments efficiently given the wide range of design conditions, a method that can complement existing CFT creep experimental methods is required.

Therefore, this study proposes an experimental method that can overcome the limitations present in existing CFT creep experiments. A long-term behavior experiment on CFT is also conducted by applying the proposed experimental method. Furthermore, a superficial creep coefficient model that considers the long-term behavioral characteristics of CFT is derived based on the experimental result. Here, the creep coefficient model is derived based on the superficial deformation data

that occurs due to the interaction of CFT concrete and steel tube. In order to verify the proposed CFT creep-experimental method and the superficial creep coefficient model of CFT, experimental results and predicted values are compared. In addition, the proposed method is also compared to the existing creep coefficient prediction models CEB-FIP 1990 (CEB-FIP., 1993) and ACI 209 (Committee&209.,) based on CFT creep experiment data compiled by previous researchers.

2 Creep Properties of CFT

2.1 Creep and Shrinkage of CFT

Creep strain means the strain increase over time when a load applied to a concrete structure remains constant. Creep strain is an important factor to consider when designing concrete structures because it affects not only the modulus of elasticity but also the strength of the structure over time. Creep strain is characterized by convergence to an almost constant value over time, and the creep coefficient of Eq. (1) is used as an index for determining the amount of creep strain. In addition, as shown in Fig. 1, the principle of strain superposition can be applied when calculating the total creep strain because the load and creep strain within the working load range of a structure are proportional:

$$\emptyset = \frac{\varepsilon_{creep}}{\varepsilon_{elastic}} = \frac{Creep\ strain}{Elastic\ strain}. \quad (1)$$

In general, creep can be classified into basic creep and dry creep depending on whether the concrete is in contact with outside air. Basic creep refers to the deformation that occurs in concrete over time assuming that there is no contact between the concrete and the outside air, and dry creep is the deformation that occurs in concrete in dry conditions other than basic creep deformation. Concrete placed in a dry environment has a greater amount of total creep than concrete placed in a wet state because basic creep and dry creep occur together (Pickett, 1942). However, for the concrete used with CFT, only basic creep is considered while dry creep is ignored because the concrete is blocked from contact with outside air due to the steel tube (Lai et al., 2019; Nakai et al., 1991; Zhang et al., 2015).

Another long-term behavioral property of concrete is shrinkage, referring to an increase in deformation over time without the action of a load. Shrinkage is classified into two types: autogenous shrinkage and drying shrinkage. Autogenous shrinkage is caused by the hydration reaction of cement. Therefore, CFT can increase autogenous shrinkage strain because high-strength concrete is often used to increase the efficiency of the CFT application, and the water-to-cement ratio is lower than that of general concrete (Larrard & Roy, 1992). Drying shrinkage is caused by the evaporation of pore water in concrete due to low humidity in the external environment. However, as mentioned above, CFT scarcely reacts with moisture and carbon dioxide in the air due to the steel tube, meaning that the amount of deformation caused by drying shrinkage is very low (Nakai et al., 1991; Terrey et al., 1994). As such, CFT has long-term behavior characteristics different from those of general concrete because the effects of drying creep and drying shrinkage can be ignored due to the structural characteristics of CFT. Another reason why the long-term behavior characteristics of CFT differ from those of general concrete is that the interaction occurs between concrete and steel tube because the steel tube restrains the concrete. Accordingly, when a load is applied to the member, a stress-redistribution effect occurs between the two materials. (Committee&209., 1997).

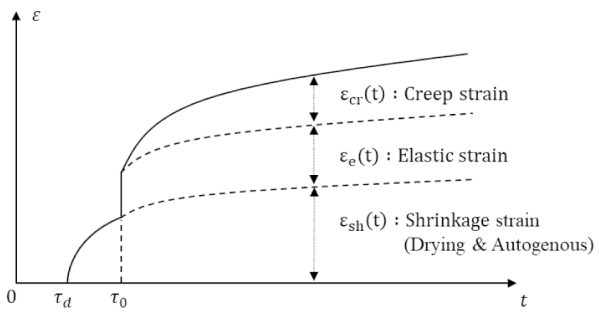

(a) Time-dependent strain of concrete

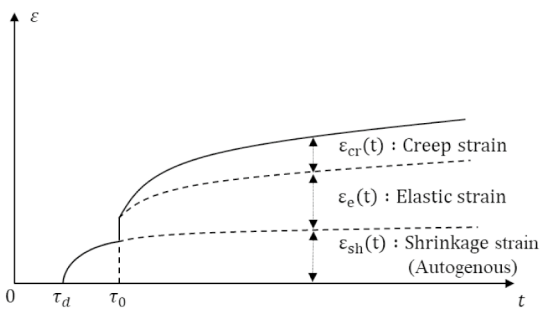

(b) Time-dependent strain of CFT

Fig. 1 Creep and shrinkage of concrete and CFT

Earlier, Terrey et al. (1994) and Ichninose et al. (2001) conducted long-term behavior experiments under the same design conditions shown in Table 1 to compare the different long-term behavior characteristics of concrete specimens and CFT specimens.

According to the experimental results of Terrey et al. (1994), the average ultimate creep coefficients of the concrete and the CFT specimen were 2.23 and 1.20, respectively, indicating that the creep coefficient of the CFT specimen was approximately 54% less than that of the concrete specimen. In addition, the drying shrinkage strain values of the concrete and the CFT specimen were 625 με and 130 με, respectively. In other words, the drying shrinkage strain generated in the CFT specimen was much lower than that of the concrete specimen. In the experimental results of Ichninose et al. (2001), the average ultimate creep coefficients of concrete and CFT specimens were 2.78 and 1.53, respectively, indicating that the creep coefficient of the CFT specimen was approximately 55% less than that of the concrete specimen. In addition, the drying shrinkage strain was about 426 με in the concrete specimen and close to 40 με in the CFT specimen. In other words, in both experiments, the deformation of CFT due to drying shrinkage was negligible and small, and creep deformation of CFT was less than half that of the concrete specimens. This indicates that CFT is relatively more effective than concrete in terms of long-term deformation.

2.2 Existing Creep Coefficient Model

When stress $f_c(t\prime)$ is applied to a concrete structure, the total strain $\varepsilon_c(t,t\prime)$ at time t is expressed as Eq. (2). Here, t' is the time the load was applied, E_{ci} is the initial elasticity modulus of concrete, and $\varphi(t,t\prime)$ is the creep coefficient:

$$\varepsilon_c(t,t') = f_c(t')\left[\frac{1}{E_{ci}(t')} + \frac{1}{E_{ci}}\varphi(t,t')\right]. \tag{2}$$

The creep coefficient is used as a method to predict creep deformation in concrete. However, it is difficult accurately to calculate the creep coefficient because it is determined by a wide variety of variables, such as the compressive strength and age of the concrete, the temperature, and the humidity level (Neville, 1970). Nevertheless, design criteria such as CEB-FIP 1990 (CEB-FIP., 1993) and ACI 209 (Committee&209.,) were used in a model to predict the creep coefficient with several design variables. Equation (3) is the CEB-FIP 1990 (CEB-FIP., 1993) creep coefficient model equation, which is presented as the multiplication of the conceptual creep coefficient and a time function representing the change in creep over time. The conceptual creep coefficient and time function are expressed here as Eqs. (4) and (5), respectively. The conceptual creep coefficient represents the change in the strength of concrete with age as a function of time based on the concrete age of 28 day. Here, $\varnothing_{RH}$ is a coefficient determined by the relative humidity, and β_H is determined as a function of the conceptual member dimension ($h = \frac{2A_c}{u}$). $\beta(f_{cm})$ is a coefficient determined by the 28-day compressive strength of concrete, and $\beta(t\prime)$ is a coefficient determined by the age of the concrete under a load:

$$\varphi_{CEB}(t,t') = \varphi_{0\_CEB} \times \beta_c(t-t'), \tag{3}$$

$$\varphi_{0\_CEB} = \varphi_{RH} \times \beta(f_{cm}) \times \beta(t'), \tag{4}$$

$$\beta_c(t-t') = \left[\frac{t-t'}{\beta_H + (t-t')}\right]^{0.3}. \tag{5}$$

Unlike other creep coefficient models, the ACI 209 (Committee&209., 1997, 2008) model predicts the creep coefficient by considering a range of different variables, particularly the degree of slump, the fine aggregate ratio, the air volume, and the concrete age and humidity. The ACI 209 (Committee&209., 1997, 2008) model presents the creep coefficient equation by multiplying the ultimate creep coefficient $\varphi\prime$ by the time function, as shown in Eq. (6). The ultimate creep coefficient is calculated by multiplying the correction coefficient based on the variables affecting the creep, as shown in Eq. (7). Here, $C_{cu}C_hC_tC_sC_f$andC_a are correction coefficients determined by the curing conditions of concrete, the relative humidity, the member thickness, the slump value,

Table 1 Long-term behavior experimental conditions and results from concrete and CFT

Refs.	Diameter and thickness (mm)	f_{ck}(MPa)	E_c(MPa)	Creep coefficient (∅)		Drying shrinkage, ε_{sh} ($\mu\varepsilon$)	
				Concrete	CFT	Concrete	CFT
Terrey et al., (1994)	∅200 × 1.5 ∅200 × 1.0	45.2	30800	2.23	1.20	625	130
Ichinose et al., (2001)	∅165.2 × 4.5 ∅165.2 × 5.0	27.8	22736	2.78	1.53	426	40

the amount of fine aggregate, and the amount of air, respectively:

$$\varphi_{ACI}(t,t') = \frac{(t-t')^{0.6}}{10+(t-t')^{0.6}}\varphi'_{ACI}, \tag{6}$$

$$\varphi'_{ACI} = 2.35\, C_{cu}C_hC_tC_sC_fC_a. \tag{7}$$

As mentioned above, it is necessary to exclude the effect of dry creep when calculating the creep coefficient of CFT (Lai et al., 2019; Nakai et al., 1991; Zhang et al., 2015). However, existing concrete creep coefficient prediction models do not reflect these structural characteristics of CFT in their design criteria, causing these models to overestimate the creep deformation of CFT. Therefore, in order to predict the creep deformation of CFT accurately, a creep model capable of properly reflecting the long-term behavior characteristics of CFT must be devised. In order to do this, it is necessary to compile a range of experimental data on the long-term behavior of CFT. However, studies that focus on creep experimentally in relation to CFT remain insufficient. Therefore, this study proposes a creep-experiment method for CFT that can be performed more efficiently with different design variables by complementing the existing experimental method.

3 Long-Term Behavior Analysis Method Considering the Stress Redistribution of CFT

3.1 Stress Redistribution of CFT

According to Nguyen et al. (2021), over time after a load is applied, stress is redistributed between the two materials of the CFT concrete and the steel tube due to creep. This stress redistribution can be explained by the concept of relaxation. As shown in Fig. 2, in the rapid load curve and the slow load curve, which represent the elastic deformation that occurs immediately after the load is applied and the long-term deformation that occurs over time after the load is applied, respectively, creep is a phenomenon in which strain increases over time when constant stress is maintained, and relaxation is a phenomenon in which stress gradually decreases over time when a constant level of strain is maintained. Creep and relaxation are closely related to one another, as when constant stress is maintained in a concrete structure, the creep deformation of concrete increases continuously over time, while the stress applied to the structure by relaxation gradually decreases over time in order to suppress the creep deformation. Therefore, when a load is applied to the CFT, the stress of the concrete gradually decreases over time due to creep, and the stress of the steel tube gradually increases because the steel tube additionally bears the reduced stress in the concrete. Therefore, the stress between the two materials is redistributed.

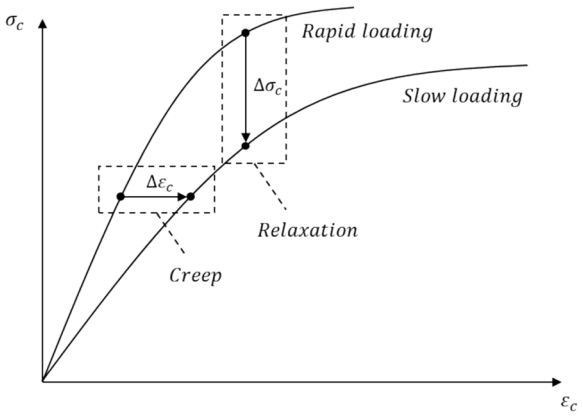

Fig. 2 Creep and relaxation of concrete

3.2 Step-by-Step Method (SSM)

A step-by-step method (henceforth SSM) is used to analyze the long-term behavior of composite structures over time by considering the stress-redistribution effect (Gilbert & Ranzi, 2010). SSM is calculated under the assumption that the creep strain applied at each time increment section does not affect other time increment sections. SSM increment the time slightly based on time point τ_0 when the load is applied and then sums the creep deformation caused by stress in each time increment section to calculate the deformation after some time has elapsed. In Fig. 3, when the incremental stress of concrete occurring between the ith time increments section is $\Delta\sigma_{\tau_i}$, the incremental values of the elastic strain and creep strain caused by stress increment $\Delta\sigma_{\tau_i}$ are calculated by the elastic modulus $E_c(\tau_i)$ and the creep coefficient $\varnothing(t,\tau_i)$ at the end of the incremented section, respectively. The total strain at the end of each time increment section is calculated as the superposition of the strains in all preceding time increment sections. The concrete strain $\varepsilon_c(\tau_{i+})$ at the end point τ_{i+} of the ith time increment section can be obtained using Eq. (8). At this time, because the effect of shrinkage can be ignored in CFT, the shrinkage strain $\varepsilon_{sh}(\tau_{i+})$ is not considered in the long-term behavior analysis:

$$\varepsilon_c(\tau_{i+}) = \frac{\sigma_{c0}}{E_c(\tau_0)}[1+\emptyset(t,\tau_0)] + \sum_{j=1}^{i}\frac{\Delta\sigma_c(\tau_j)}{E_c(\tau_j)}\left[1+\emptyset\left(\tau_{i+},\tau_j\right)\right] + \varepsilon_{sh}(\tau_{i+}). \tag{8}$$

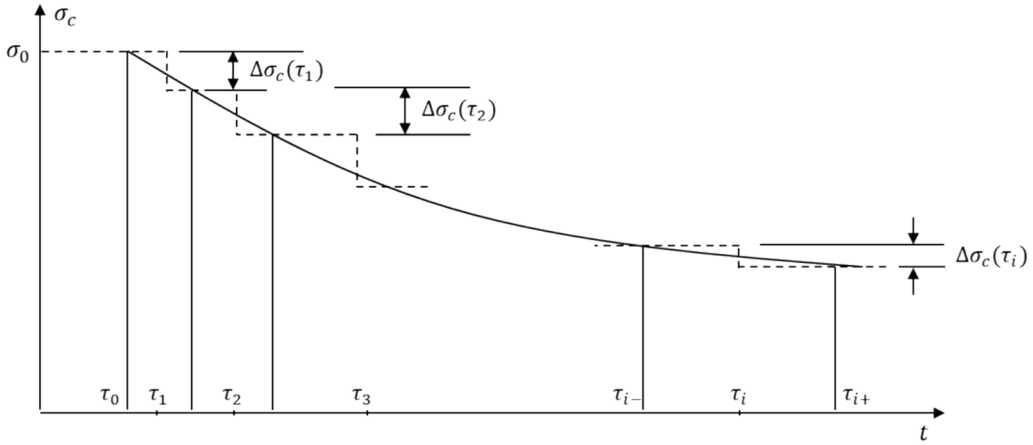

Fig. 3 Time increment of the step-by-step method

Here, σ_{c0} and $E_c(\tau_0)$ indicate the initial concrete stress and the elastic modulus, respectively, and $\varnothing(t, \tau_0)$ is the initial creep coefficient.

The initial concrete stress σ_{c0} can be calculated by Eq. (9) based on the force equilibrium equation, and the initial concrete strain ε_{c0} can be calculated by dividing the initial stress by the initial concrete elastic modulus:

$$\sigma_{c0} = \frac{P}{A_c(1+n\rho)}. \tag{9}$$

Here, n is the ratio of the elastic modulus of steel and concrete (E_s/E_c), and ρ is the steel ratio.

Under the assumption that the steel tube and concrete behave integrally, the stress loss of concrete during each time increment can be obtained based on the strain compatibility equation of Eq. (10) and the force equilibrium equation of Eq. (11):

$$\varepsilon_c(\tau_{i+}) = \varepsilon_s(\tau_{i+}), \tag{10}$$

$$\sigma_C(\tau_0)A_c + \sum_{j=1}^{i} \Delta\sigma\left(\tau_j\right)A_c + \sigma_s(\tau_{i+})A_s = P. \tag{11}$$

Here, $\varepsilon_c(\tau_{i+})$ and $\varepsilon_s(\tau_{i+})$ are the strain of concrete and steel at τ_{i+}, respectively, and $\Delta\sigma(\tau_j)$ denotes the incremental stress of concrete. σ_s is the stress of steel at τ_{i+}, and A_c, andA_s are the cross-sectional area of concrete and steel, respectively. P is the axial load applied to the member.

When Eqs. (10) and (11) are combined, the incremental stress of concrete and the stress of steel at τ_{i+} can be obtained. In addition, the strain of the steel can be determined by dividing the stress of the steel by the elastic modulus of the steel. At this time, based on the strain compatibility equation, the strain of the steel is equal to the strain of the concrete. As a result, the creep strain $\varepsilon_{cr}(\tau_{i+})$ at τ_{i+} can be calculated with Eq. (12):

$$\varepsilon_{cr}(\tau_{i+}) = \varepsilon_c(\tau_{i+}) - \varepsilon_e(\tau_{i+}) - \varepsilon_{sh}(\tau_{i+}). \tag{12}$$

Here, $\varepsilon_e(\tau_{i+})$ denotes the elastic strain of concrete.

SSM is the most accurate method among various methods for analyzing the long-term behavior of composite structures. Moreover, the amount of the stress redistribution occurring in composite structures due to creep can be predicted prior to an experiment because it can quantitatively calculate how much the stress levels in the concrete and steel change at an arbitrarily divided time step. Therefore, in this study, an experimental method was devised to illustrate the stress-redistribution effect between the concrete and the steel tube using only the concrete part of the CFT by calculating how much stress redistribution is occurring in the two materials before the CFT creep experiment is performed using SSM.

4 Proposal of the Creep-Experimental Method of CFT

The existing CFT creep-experiment method initially introduced a constant load onto the CFT specimen using a pressure plate and then periodically measured the strain using a strain gauge. However, when using this method, if the heights of the concrete and the steel tube do not precisely match at the joint surface between the CFT and the pressure plate, it may be difficult to apply the load simultaneously to the two materials. In addition, it is difficult accurately to measure the creep strain of concrete due to the structural characteristics of CFT, in which concrete fills the inside of the steel tube. It is also difficult to establish various design parameters such as the steel ratio because steel tubes are mainly manufactured as

standardized products. Therefore, in this study, a creep-experiment method for CFT called the continuous-load change creep experiment is devised to overcome the limitations of existing experimental methods used with CFT. The continuous-load change experiment is a method of simulating the long-term behavior characteristics of CFT with only the concrete part of the CFT. In other words, this method predicts the degree of stress redistribution between the concrete and the steel tube due to creep in CFT based on SSM. And researchers passively remove a load equal to the amount of stress loss generated in the concrete due to creep in the initial load. At this time, the complete surfaces of the concrete specimen must be sealed in order to apply the same outdoor air blocking effect of CFT. Here, the friction force between the two materials is ignored because the proposed method is performed under the assumption that the concrete and the steel pipe behave as one unit. Therefore, this method cannot perfectly represent the long-term behavior of actual CFT, but it can represent the superficial long-term behavior phenomenon due to stress redistribution.

The creep experimental procedure of CFT is shown in Fig. 4. First, the creep experimental conditions and the design variables of CFT are set. The conditions and the design variables include the temperature and humidity, the diameter and thickness of the CFT, and the compressive strength. The size of the initial load applied to the specimen at the working load level is then planned,

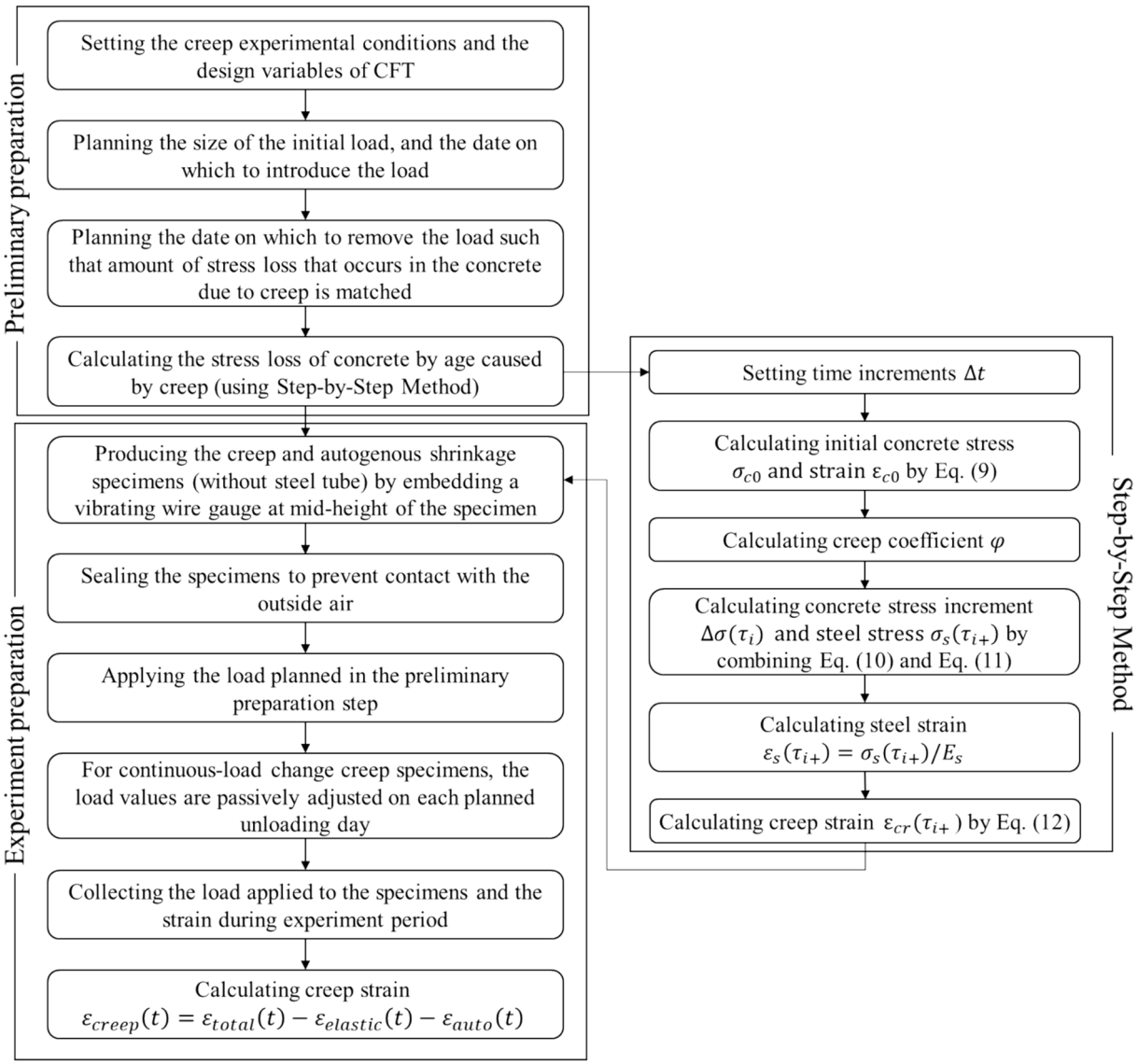

Fig. 4 Proposed CFT creep experiment procedure

as is the date on which to introduce the load and the date on which to remove the load such that amount of stress loss that occurs in the concrete due to creep is matched. When planning the load-removal day, considered the characteristics of creep, where the deformation is large at the beginning of the load and gradually decreases over time (Altoubat & Lange, 2001). Therefore, it is set to one to three days, i.e., densely, at the beginning of the experiment, with the interval gradually increasing over time. Then, preparations are completed by calculating the stress loss of concrete by age caused by creep using SSM. In this study, 50% of the concrete creep coefficient specified by the CEB-FIP 1990 (CEB-FIP., 1993) model was applied during the process of calculating SSM. This was determined based on the fact that, according to the experimental results of Terrey et al. (1994) and Ichninose et al. (2001), the CFT specimen occurred at about half of the creep deformation of the concrete specimen. In addition, for the CEB-FIP 1990 (CEB-FIP., 1993) model, when calculating the creep coefficient of concrete, the degree of deformation due to dry creep is specified as half of the total creep deformation (Kim & Jeon, 2002).

After the preliminary preparation steps are completed, a vibrating strain gauge is buried to measure creep and autogenous shrinkage strains. At this time, to ensure that the effects of drying shrinkage and drying creep can be disregarded in the same way as CFT, the entire surface of the specimen must be sealed to block contact with the outside air. When the specimens were created, the load planned in the preliminary preparation step is applied to the creep specimen. Then, for continuous-load change creep specimens, the load values are passively adjusted on each planned unloading day. The load applied to the specimens and the strain are collected from the loading date until the creep experiment is over, and the creep strain is calculated using Eq. (13):

$$\varepsilon_{creep}(t) = \varepsilon_{total}(t) - \varepsilon_{elastic}(t) - \varepsilon_{auto}(t). \tag{13}$$

Here, $\varepsilon_{creep}(t)$, $\varepsilon_{total}(t)$, $\varepsilon_{elastic}(t)$, and $\varepsilon_{auto}(t)$ are the creep strain, the total strain, the elastic strain, and the autogenous strain, respectively.

5 Methodology

5.1 Experimental Design

According to Aïtcin et al. (1998), rapid autogenous shrinkage occurs after the initial setting of concrete at the early age when the tensile strength is low because autogenous shrinkage consumes the internal mixing water during the hydration reaction of cement. CFT using high-strength concrete with a relatively small mixing quantity and small voids has a higher probability of drying inside at an early stage, which can cause greater deformation due to autogenous shrinkage. Therefore, it is important to measure the strain due to autogenous contraction during a long-term behavior experiment on CFT. For this reason, as shown in Fig. 5, during the experimental process used here, an autogenous shrinkage experiment and a creep experiment were performed independently. At this time, the creep experiment was also performed independently by dividing the continuous-load change experiment and the static load creep experiment in which a constant load is introduced at 7, 14, and 28 days of concrete age, respectively.

All specimens in the experiment were manufactured in pairs according to each design variable. The specimens were demolded and cured in a wet condition on the first day after the concrete was poured. The specimens that underwent autogenous shrinkage were manufactured under conditions identical to the creep experiment specimens, and the shrinkage strain was measured in a room with a constant temperature and humidity level. In order to ensure conditions identical for the CFT, the autogenous shrinkage specimens and the creep specimens were sealed from contact with outside air using butyl rubber, as shown in Fig. 6.

In the experiment, the concrete mixing strength was 50 MPa. The mixing design is shown in Table 2 below. The diameter and height of the specimens are 150 mm, 300 mm, respectively. The compressive strength and modulus of elasticity of the concrete were tested according to ASTM C469, and the compressive strength and modulus of elasticity of the concrete at 28 days were measured and found to be 61 MPa and 34.2 GPa, respectively. The compressive strength and modulus of elasticity of concrete by age are correspondingly shown in Table 3.

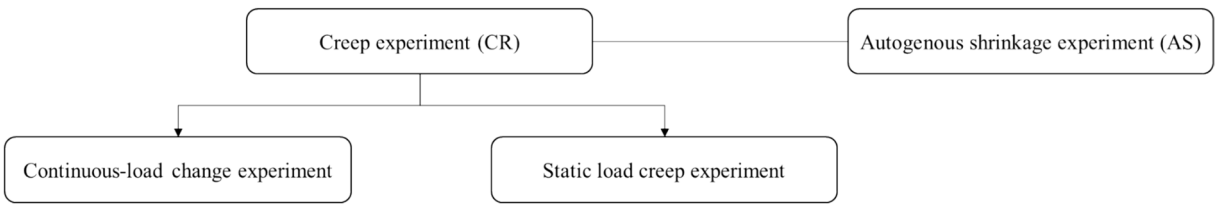

Fig. 5 Types of long-term behavior experiments

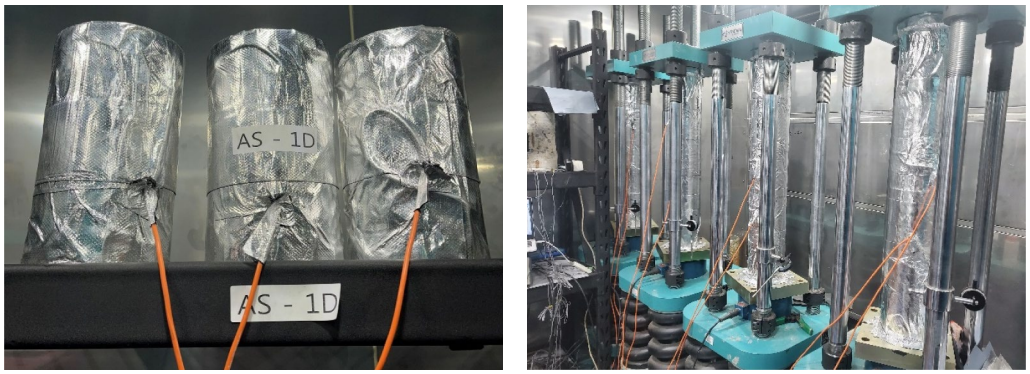

(a) Autogenous shrinkage specimens (b) Creep specimens

Fig. 6 Sealed autogenous shrinkage specimens and creep specimens

Table 2 Concrete mix design

W/B (%)	S/a (%)	Unit weight/(kg/m^3)						
		Water	Cement	Blast furnace slag	Fly ash	Coarse aggregate	Fine aggregate	Superplasticizer
33	45.8	165	225	225	50	871	736	0.8

Table 3 Compressive strength by concrete age

Age (day)	Compressive strength (MPa)				Elastic modulus (GPa)			
	Specimen #1	Specimen #2	Specimen #3	Average	Specimen #1	Specimen #2	Specimen #3	Average
7	43.7	45.5	46.2	45.11	29.0	30.8	32.5	30.8
14	56.1	55.9	55.3	55.8	29.0	30.8	33.6	33.1
28	61.4	60.8	60.9	61.0	34.1	33.6	34.8	34.2

A hydraulic cylinder with a load cell capacity of 1000 kN was used to introduce the load onto the specimens. In this case, the size of the load was about 25% of the compressive strength considering each age of the specimen and considering the actual working load of the CFT. The strain was measured by embedding one vibration-type embedded gauge per specimen at the mid-height point of the specimen. The autogenous shrinkage experiment was conducted on the concrete at one day of age, the static load creep experiment was performed on the concrete at 7, 14, and 28 days of age, and the continuous-load change creep experiment was conducted on the concrete seven days of age. In the continuous-load change creep experiment, the long-term deformation characteristics of CFT according to the steel ratio were analyzed using two steel ratios of 10% and 12%, under the assumption that the steel tube exists. All experiments lasted for 163 days, and a summary of the experimental design variables is shown in Table 4.

Fig. 7 shows the change in the load introduced onto the specimen over time in the continuous-load change creep experiment. The stress reduction in concrete due to creep was calculated for each day. In addition, the load reduction cycle was set considering the concrete deformation characteristics in which creep deformation increases rapidly at the beginning of load introduction and then becomes gradual decrease (Aïtcin, 1998). The load-removal days were set at narrow intervals of one to two days at the onset of load introduction, and at 1 month from the start of the creep experiment, the interval was as long as 30 days. At this time, the load reduction when the steel ratio is 12% is greater than when the steel ratio is 10% because as the steel ratio increases, the additional stress burden of the steel tube increases as the degree of the suppression of the properties of the concrete deformation due to creep increases. That is, the increase in the additional stress burden of the steel tube according to the increase in the steel ratio causes an increase in the stress

Table 4 Experimental design variables

Type of experiment	Specimen	Diameter (mm)	Steel ratio (%)	Age (day)	Load size (kN)	Condition
Autogenous shrinkage	AS-1D #1	150	–	1	–	No exposure to external environment
	AS-1D #2					
Static load creep	CR-7D #1	150	–	7	202	
	CR-7D #2					
	CR-14D #1		–	14	247	
	CR-14D #1					
	CR-28D #1		–	28	269	
	CR-28D #1					
Continuous load change creep	CR-7D-ρ 10-D #1	150	10	7	202	
	CR-7D-ρ 10-D #2					
	CR-7D-ρ 12-D #1		12			
	CR-7D-ρ 12-D #2					

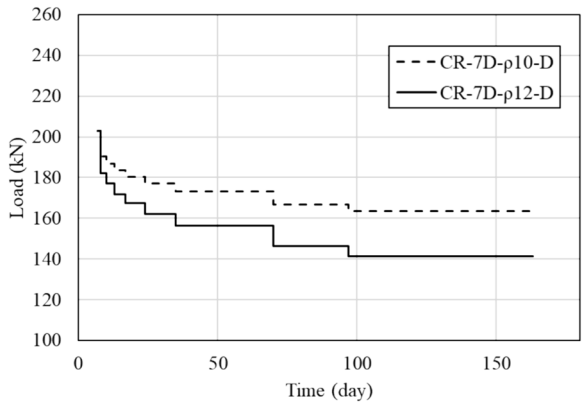

Fig. 7 Load change curve of the continuous-change load creep specimen by age

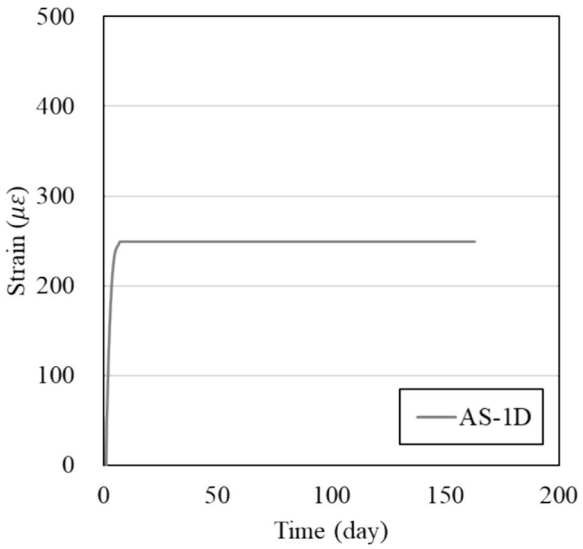

Fig. 8 Autogenous shrinkage strain by age

reduction amount of the concrete. Consequently, as the steel material ratio increases, the amount of the actual load reduction increases.

5.2 Experiment Result

In order to measure the autogenous shrinkage strain of CFT accurately, the strain was measured during the experimental period in a room with a constant temperature and humidity immediately after the concrete was poured. Fig. 8 presents the strain curve of autogenous shrinkage generated over time from the concrete age of one day. The strain increased rapidly from the first to the seventh day of age and then stabilized, converging to about 249 με on the 163rd day, which was the end of the creep experiment.

The various factors that influence the long-term behavior of concrete are internal factors determined in the design of the concrete mixture and external factors determined by the curing method and temperature used, for instance. However, because it is time-consuming and costly to conduct an experiment that takes into account all of these factors, it is important to establish the minimum design variables so as to understand the creep characteristics of general CFT. Therefore, in this study, a creep experiment with a static load was designed to identify the creep behavior characteristics of CFT according to the age of the concrete. In the static load creep experiment, the specimens were sealed to ensure conditions similar to CFT, and loads were applied at concrete ages of seven, 14, and 28 days. These specimens were correspondingly labeled as CR-7D, CR-14D, and CR-28D depending on the age of the concrete at the time of loading. The magnitudes of

the loads applied to each specimen were 202 kN, 249 kN, and 269 kN, which are 25% of the strength of each age. Fig. 9a shows the total strain curve of the specimens in the static load creep experiment. The elastic strains of the CR-7D, CR-14D, and CR-28D specimens were similarly 368 με, 398 με, and 397 με, respectively, because all specimens were introduced with the same level of the load according to the compressive strength for each age. After elastic behavior, it was observed that the rate of increase in the strain in each specimen over time differed depending on the age of the concrete when the load was introduced. The rate of increase in the strain decreased as the age of the concrete increased when the load was introduced. According to Fig. 9b, which is the creep coefficient curve by age, the creep strains of the CR-7D, CR-14D, and CR-28D specimens at 163 days were 312 με, 250 με, and 201 με, respectively; the creep strains of the CR-14D specimen and the CR-28D specimen were reduced to 20% and 36%, respectively, based on that of the CR-7D specimen. In addition, the creep coefficients at 163 days for the specimens at 7, 14, and 28 days were 0.85, 0.63, and 0.44, respectively; the creep coefficients for the CR-14D and CR-28D specimens were reduced to 26% and 48%, respectively, based on that of the CR-7D specimen.

Fig. 10 shows the total strain curve from the continuous-load change experiment. CR-7D-ρ 10-D and CR-7D-ρ 12-D are specimens in which the load equivalent to the stress loss of concrete due to creep is removed from the initial load when the steel ratio of CFT is 10% and 12%, respectively. In Fig. 10, when removing the load from the initial load, the elastic strain decreases and the creep strain increases until the next stress-removal date. Therefore, the curve of

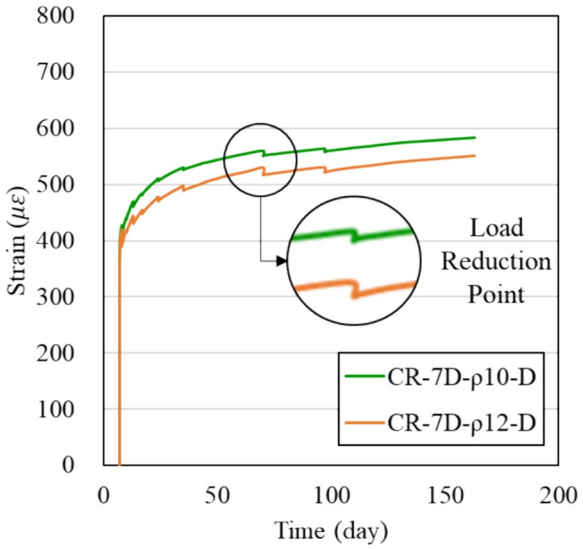

Fig. 10 Total strain in the continuous-change load creep experiment

Fig. 10 is not smooth, unlike the curve in Fig. 9, because a rapid decrease and a gentle increase are repeated whenever the load is removed passively. The initial elastic strain of the CR-7D-ρ10-D and CR-7D-ρ12-D specimen is 365 με and the creep strains are 219 με and 186 με, respectively. Hence, the amount of creep strain decreased as the steel material ratio increased. This occurred because when the steel ratio increases while the steel tube additionally bears the stress lost in the concrete due to creep, the creep deformation amount is reduced due to the suppression of the properties of the concrete that would have been further compressed due to creep deformation.

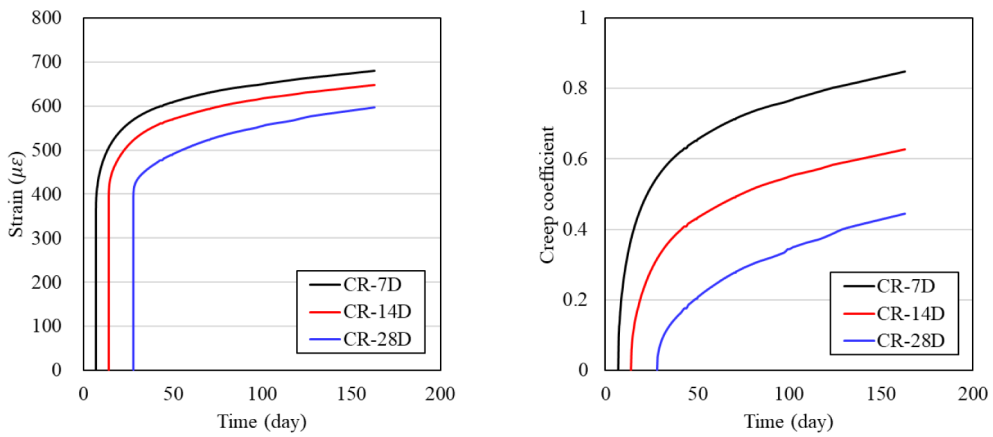

a) Time-total strain curve (b) Time-creep coefficient curve

Fig. 9 Total strain and creep coefficient in the static load creep experiment

6 Proposed and Validated Superficial Creep Coefficient Model of CFT

6.1 Proposed Superficial Creep Coefficient Model of CFT

The CEB-FIP 1990 (CEB-FIP., 1993) and ACI 209 (Committee&209., 1997, 2008) creep coefficient models were not suitable for use when attempting accurately to predict the creep that occurs in CFT because the drying shrinkage blocking effect and stress-redistribution effect of the CFT cannot be considered. Table 5 compares the creep coefficient at 163 days, representing the end date of the creep experiment, with the predicted values for the CEB-FIP 1990 (CEB-FIP., 1993) and ACI 209 (Committee&209., 1997, 2008) models and with the experimental data from this study. As a result of the comparison, both models had significant differences from the experimental results. In particular, the CEB-FIP 1990(CEB-FIP., 1993) model tended to overestimate by 1.3 times more than the ACI 209(Committee&209., 1997, 2008) model. This occurred because the ACI 209 (Committee&209., 1997, 2008) model considers the effects of various experimental variables, i.e., the relative humidity, member thickness, and slump value as well as the curing conditions when calculating the creep coefficient. Nevertheless, it can be seen that both models tend to overestimate the actual value by 1.7–3.3 times compared to the experimental data. In particular, as the concrete age increases, the difference between the experimental data and the predicted value increases. Therefore, in order to overcome the limitations of the existing creep prediction models, this study proposes a superficial creep coefficient correction model that can be applied to CFT by considering the age of the concrete based on the creep experimental data.

Table 5 Comparison of creep coefficient predicted values of existing models and experimental values

Loading age (day)	Design standard model		Exp. Creep coefficient ($t = 163$)
	CEB-FIP 1990 (CEB-FIP., 1993)	ACI 209 (Committee&209., 1997, 2008)	
7	1.95	1.44	0.85
14	1.70	1.31	0.63
28	1.46	1.18	0.44

In the static load creep experiment introduced here, during the 163-day experiment period, the creep strain data generated at concrete ages of seven days, 14 days, and 28 days were compiled. Based on the accumulated experimental data, a creep coefficient regression equation was derived for each CFT age. The superficial creep coefficient used the form of the ACI 209 (Committee&209., 1997, 2008) model, which is calculated as the product of the function of time and the ultimate creep coefficient. A regression analysis was conducted based on the experimental results of the CR-7D, CR-14D, and CR-28D specimens to derive the function of the ultimate creep coefficient according to the age of the CFT concrete. Fig. 11a is a graph predicting the ultimate creep coefficient according to the regression analysis of the experiment specimens. As a result of the regression analysis, the ultimate creep coefficients of the specimens aged 7 days, 14 days, and 28 days were 0.91, 0.68, and 0.50, respectively. Fig. 11b is the result

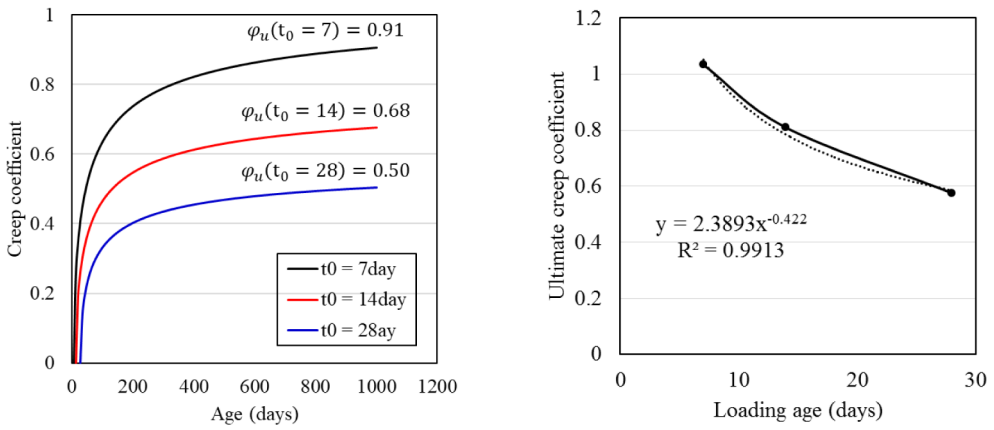

(a) Ultimate creep coefficient of CFT by age

(b) Regression equation of the ultimate creep coefficient of CFT

Fig. 11 Ultimate creep coefficient and regression equation for each age of CFT

of a second regression analysis conducted when setting the age of concrete as the x-axis and setting the ultimate creep coefficient for each age as shown in Fig. 11a as the y-axis.

Hence, the ultimate creep coefficient for each age of CFT was derived as shown in Eq. (14). Then, by multiplying Eq. (14) by the time function of the ACI 209 (Committee&209., 1997, 2008) model equation, the superficial creep coefficient estimation equation was derived. This is expressed as Eq. (15). However, it may be difficult to represent the ultimate creep coefficient of CFT concrete because the regression analysis conducted in this study used only three data for ages 7, 14, and 28 days:

$$\varphi_u = 2.389t'^{-0.422}, \tag{14}$$

$$\varphi(t,t') = \frac{(t-t')^{0.6}}{10+(t-t')^{0.6}}\varphi_u. \tag{15}$$

Here, φ_u denotes the ultimate superficial creep coefficient, and t' is the age of concrete at the time of loading.

6.2 Validation of the Superficial CFT Creep Coefficient Model

In order to verify the creep coefficient derived in the previous section and with the continuous-load change creep-experiment method, the predicted values calculated by the superficial creep coefficient and the continuous-load change experimental result were compared. Fig. 12 and Table 6 compare the values calculated with the superficial creep coefficient and the results of the continuous-load change creep experiment, and Fig. 12a, b are the experimental results assuming a steel ratio of 10% and 12%, respectively. As a result, the predicted value showed results similar to those in the experimental data. However, after 70 days of loading, a difference arose of approximately 3 to 16% between the predicted value and the experimental data. This difference is considered to be caused by errors that occur during the process of passively adjusting and introducing the load by the experimenter or errors due to temperature and humidity during the long-term behavior experiment.

Additionally, in order to verify the superficial creep coefficient model, it was compared with the CEB-FIP

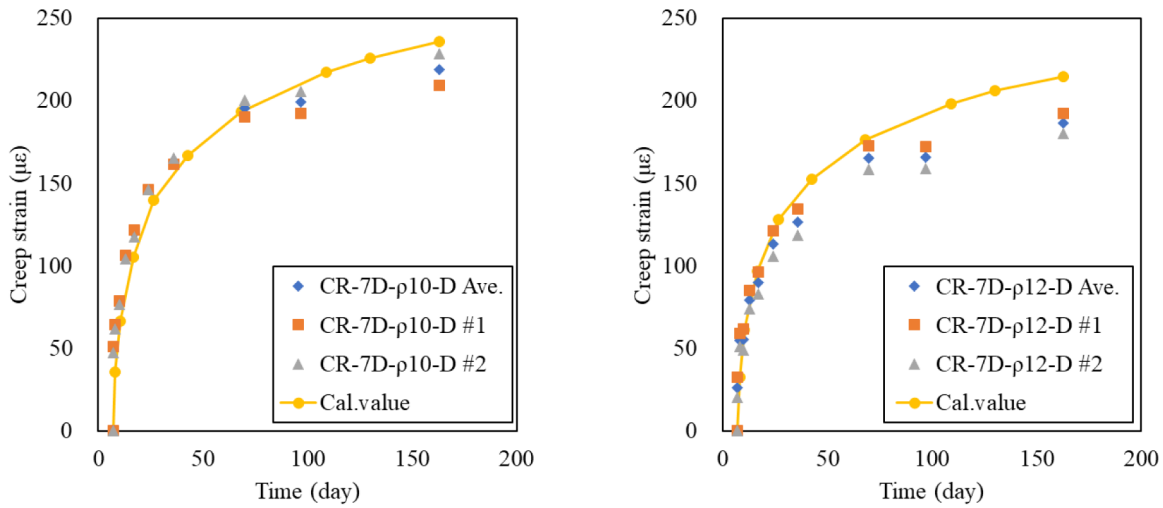

(a) Steel ratio 10% (b) Steel ratio 12%

Fig. 12 Comparison curve of the continuous-load change experimental data and the predicted values

Table 6 Comparison of continuous-load change experimental data and the predicted values

Creep strain (με)	CR-7D-ρ 10-D			CR-7D-ρ 12-D		
	Specimen #1	Specimen #2	Average	Specimen #1	Specimen #2	Average
ε_{exp}	209	228	219	192	180	186
ε_{cal}	236			215		
$\varepsilon_{exp}/\varepsilon_{cal}$	0.89	0.97	0.93	0.90	0.84	0.87

(CEB-FIP., 1993) and ACI 209 (Committee&209., 1997, 2008) models, with both of these models calculated with the drying shrinkage ignored. Table 7 presents experimental creep data for approximately 29 CFT specimens from Chen et al. (2017), Wang et al. (2011), and Geng et al. (2015). The design variables of the experiment are the loading days, the diameter and thickness of the CFT, and the compressive strength of the concrete. ε_{cr} is the creep strain that occurs in the CFT specimen. All creep strain predicted values were calculated based on SSM under identical experimental conditions for reference. As a result, the ratio of the predicted value of the superficial creep coefficient model to the experimental result showed an average of 1.09 and the standard deviation was close to 0.1, indicating that the predicted value and the experiment data were in good agreement. In this case, Fig. 13 shows some of the experimental data compared in Table 7, where it can be seen that the experimental data and the prediction curve are in good agreement over time. On the other hand, The ratio of the values predicted by the CEB-FIP (CEB-FIP., 1993) and ACI 209 (Committee&209., 1997, 2008) models and experimental values showed averages of 0.62 and 0.19, respectively, and corresponding standard deviations of 0.44 and 0.11, despite the fact that the effect of drying shrinkage was excluded. In most cases, the two models overestimated the creep strain of CFT by about 40 ~ 60% compared to the experimental results.

Table 7 Comparison of the design criteria models and the proposed model

Refs.	Specimen	t_0(days)	D (mm)	t_s(mm)	f_{cm}(MPa)	N_L(kN)	$\varepsilon_{cr,exp}$	$\varepsilon_{cr,exp}/\varepsilon_{cr,cal}$		
								Proposed	CEB	ACI
Chen et al., (2017)	CFT-0.1-CR	7	140	2	62.3	100	104	1.15	0.91	0.59
	CFT-0.2-CR	7	140	2	62.3	200	228	1.26	1.00	0.64
	CFT-0.3-CR	7	140	2	62.3	300	349	1.29	1.02	0.66
	CFT-0.4-CR	7	140	2	62.3	400	441	1.22	0.96	0.62
	CFT-0.5-CR	7	140	2	62.3	500	567	1.26	0.99	0.64
	CFT-0.6-CR	7	140	2	62.3	600	660	1.21	0.96	0.62
	CFT-C40—14–0.2-CR	14	140	2	46	182	136	1.03	0.62	0.43
	CFT-C50—14–0.2-CR	14	140	2	63	198	109	0.82	0.56	0.34
	CFT-C40—28–0.2-CR	28	140	2	46	182	123	1.25	0.66	0.43
	CFT-C40—28–0.2-CR	28	140	2	63	198	106	1.06	0.63	0.36
Wang et al., (2011)	II-1	7	140	2.62	23.6	304	0.78	0.78	0.43	0.38
	III	27	140	2.62	37.2	290	1.18	1.05	0.58	0.40
	IV	27	140	2.66	32.7	290	1.36	0.91	0.66	0.46
	V	30	140	2.6	37.2	441	1.02	1.12	0.53	0.37
	VI	30	140	2.65	32.7	441	1.26	0.92	0.65	0.45
	VII-1	29	140	2.59	37.2	515	1.00	0.92	0.52	0.36
	VII-2	29	140	2.6	37.2	515	0.90	1.03	0.47	0.32
Geng et al., (2015)	R100-T6-a	6	139.8	2.69	27.6	187	185	1.19	0.49	0.44
	R100-T6-b	6	139.2	2.7	27.6	187	158	1.39	0.42	0.38
	R100-T14-a	14	139.2	2.69	27.6	202	149	1.09	0.47	0.39
	R100-T14-b	14	139.4	2.7	27.6	202	176	0.92	0.56	0.47
	R100-T26-a	26	138.7	2.6	27.6	205	143	0.92	0.50	0.40
	R100-T26-b	26	139.1	2.74	27.6	205	162	0.81	0.58	0.47
	R50-T27-a	27	139.5	2.69	25.9	195	135	1.12	0.50	0.41
	R50-T27-b	27	138.8	2.52	25.9	195	133	1.06	0.47	0.39
	R0-T26-a	26	138.9	2.69	32.4	210	129	0.97	0.47	0.36
	R0-T26-b	26	139.3	2.66	32.4	210	123	0.93	0.45	0.34
	R100-T56-a	56	139	2.56	33.2	230	93	1.05	0.42	0.30
	R100-T56-b	56	139.3	2.67	33.2	230	99	1.13	0.46	0.33
Average								1.09	0.62	0.44
Standard deviation								0.16	0.19	0.11

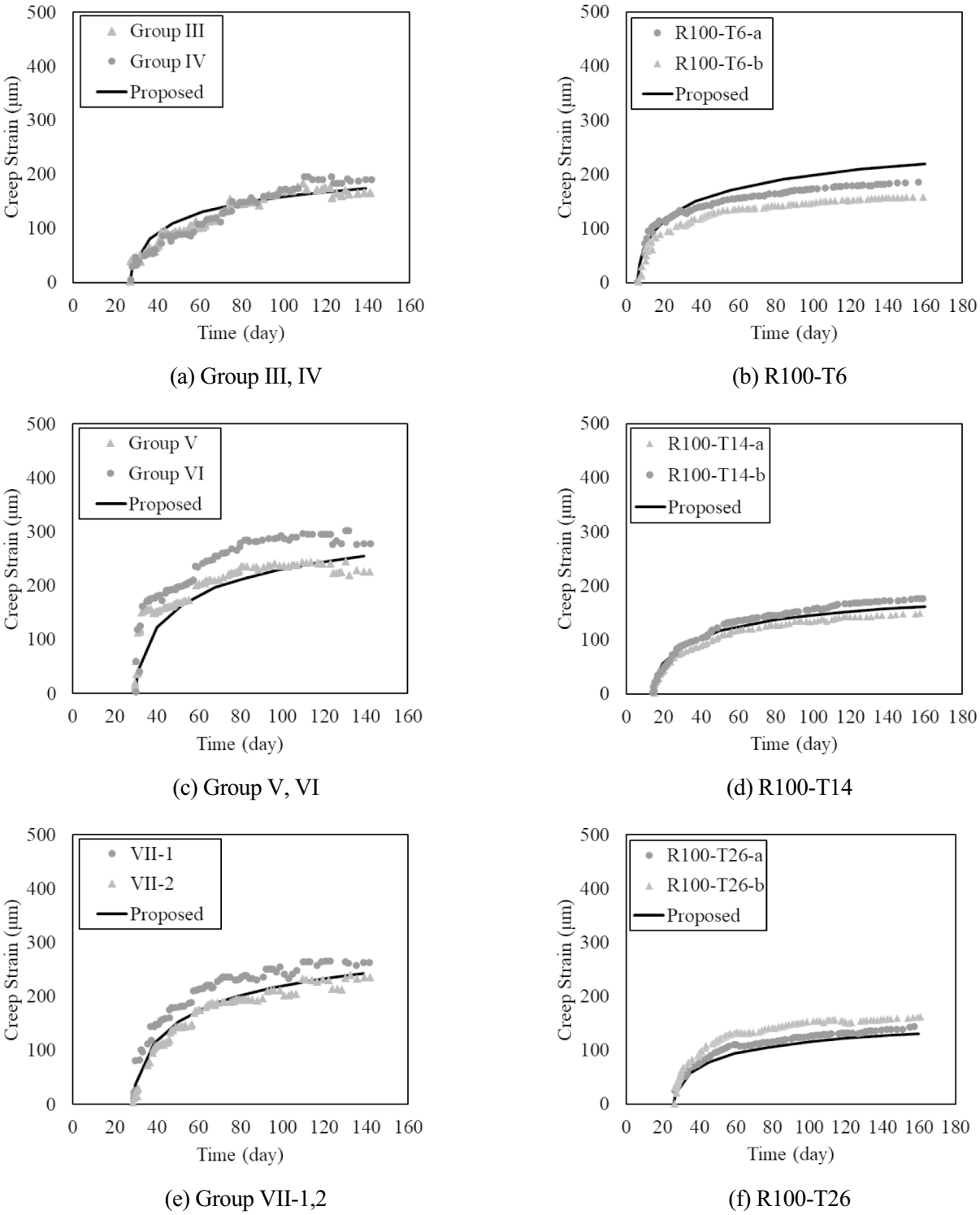

Fig. 13 Comparison curves of the experimental results and the predicted values

7 Conclusion

This study proposed a CFT creep-experiment method to overcome the limitations that affect existing CFT creep experiments. The proposed method calculates the amount of stress loss occurring in concrete due to creep before the experiment based on a step-by-step method

to consider the stress-redistribution effect that occurs between the concrete and the steel tube of the CFT. Then, after manufacturing only the concrete part without the steel tube of the CFT specimen, the load corresponding to the amount of stress loss is passively removed from the initial applied load. This is referred to as the CFT continuous-load change creep experiment. In the experiment, the autogenous shrinkage experiment and the creep experiment were performed independently. At this time, the creep experiment was also performed by isolating the continuous-load change and the static load creep experiment in which a constant load is introduced. A creep experiment that lasted for 163 days was conducted. And a superficial creep coefficient model of CFT was proposed through a regression analysis based on experimentally obtained long-term strain data. In order to verify the proposed CFT creep-experiment method and the superficial creep coefficient model, the values predicted by the superficial creep coefficient model and the CEB-FIP and ACI models were compared based on the experimental results of this study and the experimental results of previous researchers.

As a result of comparing the values predicted by the superficial creep coefficient model with the results of the continuous-load change creep experiment, the predicted values were found to be in agreement with the real experimental data. Seventy days after introducing the load, a difference of about 3–16% was shown, but this is considered to be due to errors that may have occurred during the process of passively adjusting the load. Alternatively, they may stem from the effects of the temperature and humidity. In addition, as a result of comparison, the average ratio between the CFT experimental data of previous researchers and the value predicted by the proposed model in this study was found to be 1.09. Thus, it can be seen that the proposed model predicts the creep strain of CFT well. On the other hand, the average ratios of the predicted value to the experimental data for the CEB-FIP model and the ACI model were 0.62 and 0.44, respectively, indicating that the two models overestimate the creep strain of CFT by 40–60%. Therefore, the proposed superficial creep coefficient model was verified in that it predicted the creep strain in CFT better compared to the design models, and the validity of the proposed experimental method was proved as the value predicted by the proposed model showed results similar to the continuous-load change experimental results. However, the long-term behavior experiment of CFT as conducted here utilized limited variables and there were too few experiments. Therefore, it is necessary to update the derivation formula through various experimental studies to more accurate creep coefficient prediction model of CFT. In addition, although this experiment showed results similar to the superficial behavior of CFT, the above experiment cannot completely represent the actual behavior of CFT because the stress redistribution is mechanical phenomenon. Therefore, additional research needs to be conducted to experimentally verify the stress redistribution of CFT.

Acknowledgements
Not applicable.

Author contributions
Yu-A Kim: conceptualization, methodology, writing original draft preparation, investigation. Jung-Soo Lee: experimental data measurement, collection. Seung-Hee Kwon: experimental design, preparation. Jin-Kook Kim: conceptualization, supervision, validation, reviewing and editing.

Funding
This study was supported by the Research Program funded by SeoulTech (Seoul National University of Science and Technology).

Availability of data and materials
All data generated or analyzed during this study are included in this published article [and its supplementary information files].

Declarations

Competing interests
The authors declare that they have no competing interests.

Received: 25 April 2023 Accepted: 12 May 2024
Published online: 13 September 2024

References

ACI Committee 209. (1997). Prediction of creep, shrinkage, and temperature effects in concrete structures
ACI Committee 209. (2008). Guide for modeling and calculating shrinkage and creep in hardened concrete
Aïtcin, P.-C. (1998). *High performance concrete* (1st ed.). E & FN Spon.
Altoubat, S. A., & Lange, D. A. (2001). Creep, shrinkage, and cracking of restrained concrete at early age. *Journal of ACI Material, 98*(4), 323–331.
Baweja, S., & Bažant, Z. P. (1995). Creep and shrinkage prediction model for analysis and design of concrete structures—model B3. *Journal of Material Structure, 28*, 357–365. https://doi.org/10.1007/BF02473152
Bažant, Z. P., & Wan-Wendner, R. (2015). RILEM draft recommendation: TC-242-MDC multi-decade creep and shrinkage of concrete: Material model and structural analysis. *Journal of Materials and Structures, 48*, 753–770. https://doi.org/10.1617/s11527-014-0485-2
CEB-FIP. (1993). CEB-FIP model code 1990, design code
Chen, B., Lai, Z., Lai, X., & Varma, A. H. (2017). Creep-prediction models for concrete-filled steel tube arch bridge. *Journal of Bridge Engineering*. https://doi.org/10.1061/(ASCE)BE.1943-5592.0001051
Chin, W. (2017). Developing Taiwan's concrete shrinkage formulae based on establishment and application of database.
European Committee for Standardization. (2004). BS EN 1992, Eurocode 2: Design of concrete structures—Part 1–1: general rules and rules for buildings.
fib. (2010). fib Model Code for Concrete Structures 2010, Fib Model Code Concr. Struct.
Geng, Y., Wang, Y., & Chen, J. (2015). Time-dependent behavior of recycled aggregate concrete-filled steel tubular columns. *Journal of Structural Engineering, 141*, 04015011. https://doi.org/10.1061/(ASCE)ST.1943-541X.0001241
Gilbert, R.I. & Ranzi, G. (2010). Time-Dependent behavior of concrete structures, London, United Kingdom.

Ichinose, L. H., Watanabe, E., & Nakai, H. (2001). An experimental study on creep of concrete filled steel pipes. *Journal of Constructional Steel Research, 57*(4), 453–466. https://doi.org/10.1016/S0143-974X(00)00021-3
Kim, J. H., & Jeon, S. W. (2002). CFT past, present and future-concrete filled tube. *Journal of the Korea Society for Steel Structures, 14*, 44–50.
Kwon, S. H., Kim, Y. Y., & Kim, J. K. (2005). Long-term behaviour under axial service loads of circular columns made from concrete filled steel tubes. *Magazine of Concrete Research, 57*, 87–99. https://doi.org/10.1680/macr.2005.57.2.87
Lai, X., Chen, Z. & Chen, B. (2019). Experimental study on creep of concrete filled steel tube under eccentric compression, Proceeding of ARCH international Conference on Arch Bridges.
Larrard, F.D., & Roy, R.L. (1992). The influence of mix-composition on the mechanical properties of silica-fume high-performance concrete, Proceeding of 4th International ACI-CANMET Conference on Fly Ash. Silica Fume, Slag and Natural Pozzolans in Concrete. Istanbul.
Liu, T. (2017). Developing Taiwan's concrete creep prediction formulae based on the establishment and application of database.
Nakai, H., Kurita, A., & Ichinose, L.H. (1991). An experimental study on creep of concrete filled steel tubes, Proceeding of 3rd international Conference on Steel-Concrete Composite Structures.
Neville, A. M. (1970). *Properties of concrete*. Pitman.
Nguyen, D., Lin, W., & Liao, W. (2021). Long-term creep and shrinkage behavior of concrete-filled steel tube. *Journal of Materials, 14*(2), 295. https://doi.org/10.3390/ma14020295
Pickett, G. (1942). The effect of change in moisture content on the creep of concrete under a sustained load. *Journal of ACI, 38*, 333–355. https://doi.org/10.14359/8607
Le Roy, R., De Larrard, F., & Pons, G. (1996). The AFREM code type model for creep and shrinkage of high-performance concrete, Proceeding of 4th international symposium on utilization of high-strength/high-performance concrete, Paris
Terrey, P.J., Bradford, M.A., & Gilbert, R.I. (1994). Tubular Structures, London, United Kingdom
Wang, Y. Y., Geng, Y., Chen, J., & Zhao, M. Z. (2019). Testing and analysis on nonlinear creep behaviour of concrete-filled steel tubes with circular cross-section. *Journal of Engineering Structures, 185*, 26–46. https://doi.org/10.1016/j.engstruct.2019.01.065
Wang, Y., Geng, Y., Ranzi, G., & Zhang, S. (2011). Time-dependent behaviour of expansive concrete-filled steel tubular columns. *Journal of Constructional Steel Research, 67*(3), 471–483. https://doi.org/10.1016/j.jcsr.2010.09.007
Wang, Y., & Zhao, R. (2018). Experimental study on time-dependent behavior of concrete filled steel tubes in ambient environment. *KSCE Journal of Civil Engineering, 23*, 200–209. https://doi.org/10.1007/s12205-018-1070-y
Yi, S. M., & Yuan, F. W. (2012). Creep of high strength concrete filled steel tube columns. *Journal of Thin-Walled Structure, 53*, 91–98. https://doi.org/10.1016/j.tws.2011.12.012
Zhang, D. J., Ma, Y. S., & Wang, Y. (2015). Compressive behavior of concrete filled steel tubular columns subjected to long-term loading. *Journal of Thin-Walled Structures, 89*, 205–211. https://doi.org/10.1016/j.tws.2014.12.020

Publisher's Note

Yu-A Kim Graduate student, Department of Civil Engineering, Seoul National University of Science and Technology, 232 Gongneung-ro, Nowon-gu, Seoul 01811, Republic of Korea, E-mail: kjn03221@naver.com

Jung-Soo Lee Research Professor, Hybrid Structural Testing Center, Myongji University, 34 Geobukgol-ro, Seodaemun-gu, Seoul 17060, Republic of Korea, E-mail: jung86ss@gmail.com

Seung-Hee Kwon Professor, Department of Civil and Environmental Engineering, Myongji University, 34 Geobukgol-ro, Seodaemun-gu, Seoul 17060, Republic of Korea, E-mail: kwon08@mju.ac.kr

Jin-Kook Kim Ph.D., Associate Professor, Department of Civil Engineering, Seoul National University of Science and Technology, 232 Gongneung-ro, Nowon-gu, Seoul 01811, Republic of Korea, Phone: +82 2 970 6578, Fax: +82 2 948 0043, E-mail: jinkook.kim@seoultech.ac.kr